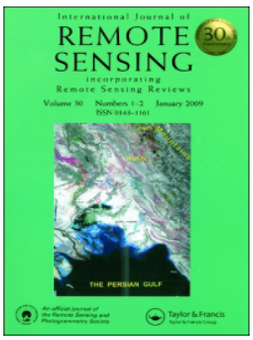

International Journal of Remote Sensing

ISSN: (Print) (Online) Journal homepage: https://www.tandfonline.com/loi/tres20

Effect of varied unmanned aerial vehicle laser scanning pulse density on accurately quantifying forest structure

Matthew J. Sumnall, Timothy J. Albaugh, David R. Carter, Rachel L. Cook, W. Cully Hession, Otávio C. Campoe, Rafael A. Rubilar, Randolph H. Wynne & Valerie A. Thomas

To cite this article: Matthew J. Sumnall, Timothy J. Albaugh, David R. Carter, Rachel L. Cook, W. Cully Hession, Otávio C. Campoe, Rafael A. Rubilar, Randolph H. Wynne & Valerie A. Thomas (2022) Effect of varied unmanned aerial vehicle laser scanning pulse density on accurately quantifying forest structure, International Journal of Remote Sensing, 43:2, 721-750, DOI: 10.1080/01431161.2021.2023229

To link to this article: https://doi.org/10.1080/01431161.2021.2023229

INTERNATIONAL JOURNAL OF REMOTE SENSING
2022, VOL. 43, NO. 2, 721–750
https://doi.org/10.1080/01431161.2021.2023229

Taylor & Francis
Taylor & Francis Group

Effect of varied unmanned aerial vehicle laser scanning pulse density on accurately quantifying forest structure

Matthew J. Sumnall[a], Timothy J. Albaugh[a], David R. Carter[a], Rachel L. Cook[b], W. Cully Hession[c], Otávio C. Campoe[d], Rafael A. Rubilar[e], Randolph H. Wynne[a] and Valerie A. Thomas[a]

[a]Department of Forest Resources and Environmental Conservation, Virginia Polytechnic Institute and State University, Blacksburg, VA, USA; [b]Department of Forestry and Environmental Resources, North Carolina State University, Raleigh, NC, USA; [c]Biological Systems Engineering Department, Virginia Polytechnic Institute and State University, Blacksburg, VA, USA; [d]Departamento de Ciências Florestais, Universidade Federal de Lavras, Lavras, MG, Brazil; [e]Departamento de Silvicultura, Universidad de Concepción, Cooperativa de Productividad Forestal, Facultad de Ciencias Forestales, Concepción, Chile

ABSTRACT

Airborne laser scanning (ALS) is increasingly used to estimate various forest characteristics. Technological improvements in unmanned aerial vehicles (UAVs) and drone laser scanning (DLS) sensors have permitted the acquisition of high pulse density datasets. There is an assumption that higher pulse densities yield greater accuracies in estimating forest characteristics. In this study, we investigated the effect of pulse density (.25, .5, 1, 5, 10, 50, 100 and 300 pulses m^{-2}) on the ability to delineate individual tree crowns (ITCs) and estimate ITC height and crown horizontal diameter, in addition to plot-level leaf area index (LAI). The current study took place in an experimentally varied *Pinus taeda* L. forest, which included three stem densities: (i) 618; (ii) 1236; and (iii) 1853 trees per hectare (TPH). ITCs were classified directly from the DLS point cloud for each of the pulse densities. The correct delineation of ITCs relative to field tree-coordinates was relatively consistent (±5%) for pulse densities of 5 to 300 pulses m^{-2}. ITC delineation accuracy decreased with lower pulse densities. Planting stem density did impact ITC delineation accuracy. Higher pulse densities, plots with 618 TPH correctly classified ~88% of ITCs, and plots with the 1853 TPH correctly classified ~50% of ITCs. Estimates of tree height were largely unaffected by changes in tree density. Root mean square error (RMSE) for tree height varied from .5 to 2.5 m at pulse densities of 300 to .25 pulses m^{-2}, respectively. Estimates of crown horizontal diameter varied with regard to both pulse and stem density from 1.2 (300 ppm^{-2} and 1853 TPH) to 4.2 m (.25 ppm^{-2} and 618 TPH). RMSE varied among stem densities from .6 to 1.2 m as pulse density decreased. There was significant difference in ITC delineation accuracy, particularly when considering stem density, and the estimates of tree height and crown horizontal diameter among the DLS pulse densities used. The accuracy of

ARTICLE HISTORY
Received 4 September 2021
Accepted 22 December 2021

Keywords
LiDAR; precision forestry; LAI; loblolly pine; silviculture; individual tree crown delineation; remote sensing

CONTACT Matthew J. Sumnall msumnall@vt.edu Department of Forest Resources and Environmental Conservation, Virginia Polytechnic Institute and State University, 228 Cheatham Hall, Blacksburg, VA 24061, USA
Supplemental data for this article can be accessed https://doi.org/10.1080/01431161.2021.2023229.

predicted LAI was largely unaffected by changes in pulse density, when pulse density was above .5 pulses m^{-2}. There was little or no difference in estimates of LAI at these pulse densities. Our results suggest that low-density DLS data may be capable of estimating plot-level forest metrics reliably in some situations, however once the analysis scale is reduced to the individual-tree-level, the influence of pulse density is more substantial. The results here provide guidance to forest managers who must balance metric estimation accuracy and price when planning new ALS or DLS acquisitions.

1. Introduction

1.1. Airborne laser scanning

Airborne laser scanning (ALS) remote sensing provides a rapid and effective means of acquiring many forest metrics that are otherwise measured with great labor cost from the ground (Hummel et al. 2011). Thus far, however, ALS is not readily adopted due to acquisition cost. Many questions still remain regarding the specifications needed to create the most accurate forest assessments for the least investment. A number of studies have attempted to assess this issue with regard to conventional ALS acquisitions at the plot-level (Jakubowski, Guo and Kelly 2013a; Kamoske et al. 2019;; Silva et al. 2017; Shao et al. 2019). Jakubowski, Guo and Kelly (2013a) found that metrics related to coverage (e.g. canopy cover) were more sensitive to low pulse densities (<20 pulses m^{-2}) when compared to metrics such as tree height, shrub height, and statistical estimates of diameter at breast height and basal area, which were relatively unaffected until pulse density was reduced to below 1 pulse m^{-2}. High pulse densities (>20 pulses m^{-2}) are thought to be more accurate (Shao et al. 2019). Likewise, Silva et al. (2017) observed more accurate digital terrain models when pulse density was highest (where tested densities ranged from 12 to .2 pulses m^{-2}). Features of interest which are smaller than the plot-level, e.g. the individual-tree-level, in particular, are subject to more uncertainty regarding a minimum required pulse density for the specific detection of that feature (Kamoske et al. 2019). The assessment of features which are smaller than the plot-level therefore presents a potential problem when considering the effects of pulse density.

Recent technological developments had enabled unmanned aerial vehicles (UAVs) as a viable remote sensing platform which have the capability to capture very high-resolution data (Wallace et al. 2012). The estimation of forest vegetation structure metrics has been demonstrated using drone laser scanning (DLS) (Sankey et al. 2017) and provides comparable products to ALS. DLS therefore can provide high point-density datasets which can be subsampled to lower densities.

1.2. Delineation of individual tree crowns

Individual tree crown (ITC) delineation is critical for assessing forest metrics since accurate estimation of ITC metrics are necessary for estimating individual-tree attributes which could be used to supply tree-level inputs to existing frameworks for growth and yield modeling, fire behavior, and habitat classification (Kaartinen et al. 2012; Jeronimo et al. 2018), improving the potential for decision making. For these ITC approaches, it is worth noting that ITCs located in

the dominant or codominant canopy are always detected better than sub-canopy trees, and the disparity grows with increasing stand height (Vauhkonen et al. 2012; Jakubowski et al. 2013b; Eysn et al. 2015). In particular, canopy structural arrangement has been found to play a considerable role in the accuracy of ITC delineation methods, to a greater degree than species or species compositions (Wang et al. 2016).

The delineation of ITCs is possible when using small-footprint (i.e. <1 m) ALS data. There are several methods which function on an ALS-derived raster canopy height model (CHM – an interpolated surface which contains estimates of height of vegetation (Brandtberg et al. 2003; Popescu and Wynne 2004;; Eysn et al. 2015; Wang et al. 2016). Methods have been developed to delineate ITCs directly from ALS point cloud returns which could potentially improve delineations (Kaartinen et al. 2012; Ferraz et al. 2016; Wang et al. 2016). Li et al. (2012), for example, demonstrated a method to classify ITCs within the point cloud by exploiting the relative horizontal spacing between trees to group ALS returns, detecting up to 86% of trees. As suggested in Yao et al. (2014), however, various parameters can influence the accuracy of results, in particular the pulse density available.

Improving the accuracy of ITC delineations may be possible with new methodologies that include higher pulse densities. Many of the available methods are applied to an ALS derived CHM surface.

The presence of individual or clusters of trees have been inferred using multiple method utilizing some variation on object recognition, local maxima finding or watershed algorithms (Brandtberg et al. 2003; Popescu and Wynne 2004; Popescu, Wynne and Scrivani 2004; Kaartinen et al. 2012; Jing et al. 2012; Eysn et al. 2015; Wang et al. 2016). The authors indicated that there was a great deal of variation in the capabilities of each algorithm depending on application context, and most importantly the performance was related to the quality and spatial resolution of the input CHM, which was dependent on the available pulse density of the ALS data. Few studies have evaluated these methods with regards to variable pulse densities (e.g. Wang et al. 2016), which concluded that for methods of ITC delineation using ALS returns, the density of the point cloud data has a significant influence on the detection rate. Therefore, additional investigation was warranted to improve the methodology for estimating ITC and assessing their accuracy.

1.3. Estimating tree height and crown width

Depending on which forest structural feature is being estimated, there are varying degrees of accuracy in their measurement, in addition to what is considered acceptable accuracy for management purposes. Vegetation height measurements have been reported to be accurate even with vegetation of short stature (~1 m), at least in areas of relatively flat terrain (Lefsky et al. 2002). For trees where the crown tapers to a point, such as in many conifer species, an ALS dataset of a high pulse density (i.e. >10 ppm^{-2}) is often necessary for the most accurate height estimates (Jakubowski et al. 2013a). A number of studies have explored the accuracy of ALS for ITC-level height estimation, with root mean square errors (RMSEs) between 1.13 to 2.05 m (Suárez et al. 2005; Kwak et al. 2007; Moe et al. 2020). Variation in accuracy among these structural features may depend on the ecosystem and tree species being measured, in addition to the complexity of the topography in the area (Silva et al. 2017) and the ALS acquisition characteristics.

Few studies have reported estimates of crown horizontal width from ALS derived ITCs. Many of these approaches create ITC objects from a raster CHM derived from ALS, and apply a segmentation approach for the delineation of the horizontal extent of an ITC, with RMSEs between .93 to 2.08 m (Falkowski et al. 2006; Popescu and Zhao 2008; Kato et al. 2009). As evidenced by previous research, crown horizontal width is capable of being quantified, yet, potentially, with greater accuracy.

1.4. Estimation of leaf area index

Leaf area index (LAI) is defined as the total one-sided leaf surface area per ground surface area (Chen and Black 1992). LAI is an important metric for forest mensuration as it is correlated with the capacity of vegetation to intercept light and, subsequently, potential productivity (Cannell 1989; Linder 1987). A substantial number of ALS studies have attempted to use 3D structural information to estimate LAI at the plot-level (Gitelson et al. 2002). Various light penetration indices have been developed to estimate forest LAI based on ALS observation, calculated either using return count or intensity (Barilotti, Turco and Alberti 2006; Hopkinson and Chasmer 2009; Morsdorf et al. 2006; Solberg et al. 2009; Sumnall et al. 2021). Pulse densities in these studies range from 5 to 30 pulses m^{-2} (Alonzo et al. 2015; Heiskanen et al. 2015; Sumnall et al. 2021), where RMSE range from .01 to .69 m^2 m^{-2} over a range of environmental contexts. By their nature, these approaches are dependent on the density and structure of vegetation *in situ* and a pulse density high enough to return data from the lower vertical strata of a forest plot is required to ensure accuracy. Lower pulse densities (between 2 and 10 pulses m^{-2}) can yield acceptable LAI accuracy in estimates for specific acquisition contexts (Almeida et al. 2019). Based on these studies, training models for local acquisition specifications are often used. Such models are not typically directly transferable to other contexts (Latifi and Koch 2012). In Sumnall et al. (2021), however, methods were developed using multiple sites and ALS acquisitions for managed loblolly pine (*Pinus taeda* L.) dominated sites, and no issues related to location were encountered. Fekety et al. (2018) demonstrated that models can be transferred between ecologically similar forests and, thus, an evaluation of ALS-derived LAI estimates across a range of pulse densities and stem densities could be conducted and potentially guide future acquisitions.

1.5. Goal and objectives

The overall goal of this study was to evaluate the effects of a range of DLS pulse densities under a variety of crown architectures (sizes and leaf densities) and stand conditions on the estimations of various forest metrics. We utilized an 8-year old, experimentally varied loblolly pine study site which possessed different genetic entries under various spacings and management intensities for this analysis. Given these conditions, this site served as an ideal location to test the effect of varied pulse densities in accurately quantifying structural attributes in a loblolly pine plantation. The specific objectives were therefore to:

(1) Classify ITCs and estimate height and crown diameter, in addition to estimating LAI at the plot-level from a normalized DLS point cloud using different pulse densities;
(2) Evaluate the accuracy of ITC delineations, ITC height and crown diameter estimates and plot-level LAI for each of the pulse densities tested;

(3) Estimate the minimum pulse density required for ITC delineation and the estimation of ITC height, ITC width, and plot-level LAI.

The datasets used in this research study are described in Sections 2.1.1 and 2.2, which provide details on the field study sites and the DLS reference data, respectively. Section 2.3.3 provides a description of the pulse densities evaluated. Sections 2.4.4–2.8 provides a description of the ITC delineation method, the LAI estimation method and statistical analysis implemented. In Section 3, the results are presented, while Section 4 contains the discussion. Finally, conclusions are presented in Section 5.

2. Materials and methods

2.1. Study site and field sampling

The study site was located in Bladen Lakes, North Carolina, USA (34°49′49.63″N, 78°35′18.52″W), and established in 2009 to investigate intensive management in optimizing loblolly pine production. The split-split plot experimental design contains three replications of six genotypes (four clones, one control pollinated and one open-pollinated) of loblolly pine, and two levels of silviculture, planted at three initial densities where all densities had the same distance between rows (3.66 m), summarized in Table 1 (Yáñez et al. 2015; Yáñez, Seiler and Fox 2017).

There was a total of 108 experimental units with 63 trees in each (7 rows of 9 trees each). All plots received chemical site preparation in November 2008. The silvicultural levels were: (*i*) operational and (*ii*) intensive. Operational silviculture included a one-time herbaceous weed control during the first growing season. Intensive silviculture treatments were designed to achieve near maximum growth for the site-soil and climatic conditions, and included herbaceous weed control in the first year, plus additional competing vegetation control in years 1, 2, 5, and 7, and fertilization in years 1, 2, and 5. Trees were planted in February 2009 and treatment effects provided a range of tree heights, distributions of canopy elements, crown sizes, and crown closures. The use of the six different genotypes of loblolly pine was intended to maximize within group homogeneity (i.e. one genotype was deployed per split-split plot), and ensure there were crown structural differences among groups via the deliberate selection of different crown ideotypes.

In January 2017, we measured 6,804 individual-tree stems. For each live tree, we measured GPS location and survival using the Trimble R8 instrument at the time of planting. The expected positional accuracy was expected to be less than 1 cm (Trimble 2003). For ~40% of stems (25 of 63) in the measurement plots (2,700 for all plots), we measured tree top height and crown horizontal diameter in the field. Tree top height was recorded using a Vertex hypsometer. The associated error of tree height via hypsometer

Table 1. Field plot attribute summary.

Stem planting density	Trees per hectare	Within row spacing (m)	Plot size (m^2)
Low	618	4.42	1019
Medium	1,236	2.21	510
High	1,853	1.47	339

was assumed to be .2–.3 m (as in Vasilescu 2013). Crown measurements were taken within and across row, and the largest diameter was recorded, as defined by Schomaker et al. (2007). This was accomplished using a measuring tape held at a point located under the edge of the crown of the measurement tree in two perpendicular directions. The end of the crown was defined as the perimeter that was visible from the ground directly beneath. The error of measuring crown diameter on the ground, to the full extent of the individual crowns, is estimated to be at .6–.9 m (Popescu, Wynne and Nelson 2003).

All field plot LAI measurements ($n = 108$) were made via nondestructive optical means using a LI-COR LAI 2200 plant canopy analyzer (LI-COR 2012) in February 2017. A total of 10 readings were recorded within each field plot via transects. Field measurements of LAI below the canopy were taken throughout the day during clear sky conditions at 1.0 m above ground. A 10° view cap was used. The calculations of LAI per plot were produced through the LI-COR FV-2200 (version 2.0) software, with no clumping corrections applied. In order to account for plot size, ring five measurements were removed for the medium and high planting density plots (as described in LI-COR 2012). The correction for light scattering (as presented in Kobayashi et al. 2013) was implemented for all measurements. Plot-level readings were averaged after excluding records with transmittance values >1. Simultaneous above- and below-canopy readings were recorded and synchronized prior to LAI calculation (Welles and Norman 1991).

2.2. DLS data acquisition and pre-processing

Discrete return DLS data was acquired in August 2017 to coincide with peak-leaf area conditions. The UAV platform was a Vapor-35 helicopter (AeroVironment, Simi Valley, CA, USA) with a YellowScan Surveyor Core lidar unit (Monfeerier-sur-Lez, France). The DLS unit consists of a Velodyne VLP-16 laser scanner (Velodyne, San Jose, CA, USA) and a GNSS-inertial Trimble APPLANIX APX-15 (Trimble, Richmond Hill, ON, Canada). The DLS system recorded up to two returns per laser pulse. Horizontal and vertical beam divergence was 3 and 1.5 mrad, respectively (Velodyn 2019). Horizontal and vertical laser footprint size at a distance of 50 m was reported as 26.4 and 17.0 mm, respectively. The wePilot1000 flight control system and the weGCS ground control system software (weControl SA, Courtelary, Switzerland) were used for flight planning. Data were recorded to the following specifications:

- a laser pulse density (312 to 498 pulses m^{-2});
- ≤60° scan angle on either side of nadir;
- altitude of 60 m (relative to take-off location);
- a 50% flight-line overlap.

Ground control was provided using a real-time kinematic geographic positioning system (RTKGPS, Topcon GR-3). The manufacturer reported precision was ≤10 cm and positional accuracy was ≤5 cm. The coordinate reference system was set to UTM zone 17N, and both horizontal and vertical units were set to meters. UAV flight control and pre-processing were handled by Applanix POSPac UAV/MMS and YellowScan CloudStation software.

A number of pre-processing steps were required before metrics could be derived from the DLS data for analysis. All of these steps were performed using the LasTools software (version 180812) (Isenburg 2019). Noise points were classified and removed if they were over 2 m away from any neighboring point. Above-ground heights were calculated by

subtracting the heights of non-ground classified points from a surface determined by a triangular irregular network created from points classified as ground. Those DLS returns <.2 m above-ground were considered to be from the ground, while returns above this threshold were classified as vegetation (either understory or canopy).

Analysis of the DLS dataset was then completed using R software (version 4.0.3.) (http://www.r-project.org/). The LiDR (version 3.1.1; Roussel et al. 2020) and datatable (version 1.12.8; Dowle and Srinivasan 2019) packages were used to read and operate on LAS format files. Geographic information system functions, such as clipping point cloud data for field plot locations, were provided by the sp (version 1.4–2; Bivand et al. 2013), rgeos (version .5–3; Bivand and Rundel 2021) and rgdal (version 1.5–8; Bivand et al. 2021) packages. The dbscan package (version 1.1–5; Hahsler, Piekenbrock and Doran 2019) was used for clustering points based on relative distance to their neighbors. The MASS package (version 7.3–53; Venables and Ripley 2002) was used for 2D kernel density analysis. The Raster package (version 3.4–5; Hijmans 2020) was used for raster manipulation. The ForestTools package (version .2.1; Plowright and Roussel 2020) was used for raster-based watershed segmentation. Linear mixed-effects models, and the assessment of least-squares means utilized the following packages: lme4 (version 1.1–27; Bates et al. 2014); lmerTest (version 3.1–3; Kuznetsova et al. 2017) and lsmeans (version 2.27–2; Lenth 2016). The multcomp package (version 1.4–17; Hothorn et al. 2008) was used to evaluate binomial generalized linear mixed-effects models. Functions were also used from the car package (version 3.0–10; Fox and Weisberg 2018).

The field plot location polygons were increased in size by 5 m via buffering operation, so as to include the entirety of all crowns within each plot. A point-cloud subset was extracted for each buffered field plot location.

2.3. Defining DLS pulse densities

The processed DLS point-cloud data that intersected with each field plot horizontal extent were systematically reduced to assess the impacts of fewer pulse densities on the accuracy of estimates of DLS-derived structural features. The DLS data provided a pulse density in excess of 300 pulses m^{-2} for all field plots in the study site. A consistent maximum of approximately 300 pulses m^{-2} was available across all plots and thus serve as the highest pulse density used here. In order to emulate different acquisition specifications, a number of lower pulse density values were subsampled from the original data to those stated in Table 2. Subsampling was achieved by first classifying individual DLS pulses using GPS time (recorded during the acquisition). These pulses were then subsampled systematically via GPS time in order to ensure uniform densities for each plot. The following processes were applied separately to each pulse density dataset to derive estimates of structural features.

2.4. Individual tree crown delineation

Initial ITC delineations were provided by implementing the methods outlined in Li et al. (2012). The method uses the spacing between the tops of trees to identify and group points into individual trees. Tree crowns were classified iteratively, starting from the tallest return. In order to improve segmentation accuracy an adaptive spacing threshold (dt) was used, where: dt = 1.25 and 1 m was set as the horizontal search distance between returns when return heights

Table 2. Summary of DLS pulse densities produced.

Iteration	Pulse density m^{-2}
1	300
2	100
3	50
4	10
5	5
6	1
7	0.5
8	0.25

were ≥10 and <10 m, respectively (Li et al. 2012) regardless of pulse density. This height threshold was selected as this was the 50th percentile of field measured individual tree heights, rounded to the nearest integer. We assume that horizontal tree spacing at the upper level is equal to or greater than 1.47 m (see Table 1) and that the taller trees likely have greater spacing and hence larger crown sizes. Minimum spacing was set to 1 m horizontally. Shape index rules were not implemented here. Heights below 1 m were considered too small and were excluded.

2.5. Refining individual tree crown delineation algorithm

The ITC classifications were further refined in order to account for parts of neighboring tree crowns erroneously being included. All returns below 1 m from the ground were ignored for this part of the method. For each of the ITC classifications, a 3D density-based spatial clustering of applications with noise (DBSCAN) approach was used. This technique groups together points that were closely packed together and marks outlier points that lie alone or in low-density regions. These clusters were defined by an allowed search radius (i.e. epsilon neighborhood) around each point. DBSCAN was sequentially applied to the classified returns of each unique ITC class to find out if it was composed of multiple non-connected parts. The use of different pulse densities required the scaling of the DBSCAN search radius. Eight sample datasets were extracted for each pulse density, for a single consistent tree location. A search radius was determined manually for each sample dataset. These settings were used to create a linear model. The DBSCAN search radius was scaled by pulse density and was defined using the following linear model:

$$eps = -0.0014 \times pulse_{density} + 1.0164 \quad (1)$$

where *eps* was the size of the search radius of the epsilon neighborhood in meters and $pulse_{density}$ was the pulse density per meter-squared existing within the current plot subset. If multiple clusters were classified here, the cluster containing the return with the largest height (assumed to be the tree top), was considered to be the ITC, and other clusters were then reclassified as a temporary class.

A convex-hull was calculated around each of the ITC clusters and the horizontal area of each ITC was calculated. If the hull area exceeded or equaled 5 m^2, the horizontal kernel density raster surface (with a bivariate normal kernel) of points was calculated for the horizontal distribution of returns in that cluster. This method was intended to identify clusters of tree crowns within one ITC classification (Figure 1(a)). The resultant 2D raster

image created was 100 × 100 cells in size regardless of the horizontal extent of the classified returns of a single ITC (Figure 1(b)). The kernel bandwidth was left as default, as defined in Venables and Ripley (2002; eq. 5.5). Local maxima coordinates were located on this raster image using a moving window size of approximately one-tenth of the total size of the raster area (33 × 33). If multiple maxima were found, we applied a marker-controlled watershed segmentation applied to the raster image in order to give the general outlines of the occupied areas – we assumed this corresponded to the extent of the crown cluster. The cluster containing the highest return height was assumed to contain the tree top, and was termed the main cluster. A transect line was then created from the maxima location in the main cluster to the location of each of the other maxima (Figure 1(b)). The raster cells which intersected this line were then extracted and analyzed (Figure 1(c)). We assumed that a separation between these potential crown objects would

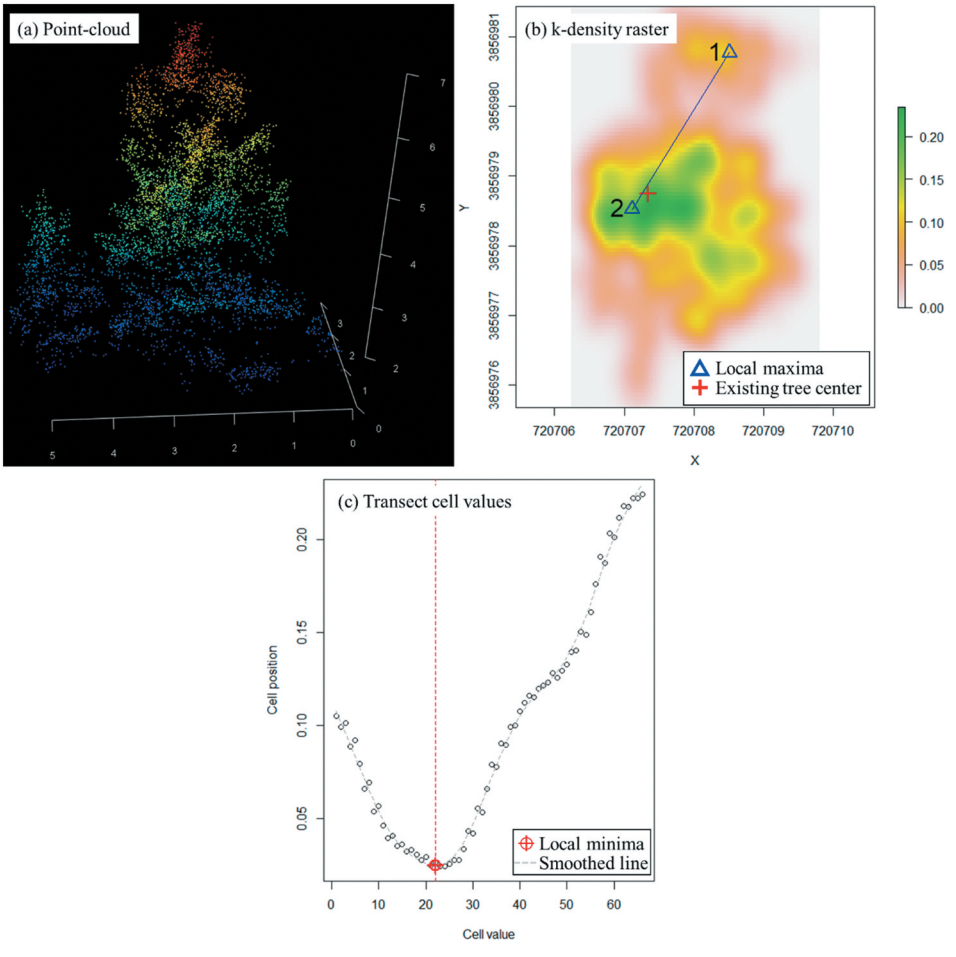

Figure 1. (a) An example cluster of two potential tree crowns classified as an individual tree crown (ITC) object, where a much smaller crown neighborhood a larger one. (b) A 2D kernel density raster produced from the returns classified as part of the current ITC. Local maxima are calculated and the closest to the 2D location of the tree top is classified as the main crown. Transects are calculated from the main to any neighboring maxima. (c) An example of raster cells intersecting the transect-line.

be characterized by a general U-shape (i.e. large values at either end of the transect and a single minimum somewhere between them). If this shape was observed, and if the maximum density/cell value belonging to the non-center cluster had an equal to or greater density/cell than the main cluster (with a local minimum in-between), the non-main maxima was considered as separate. A watershed segmentation was them implemented on the main and all separate maxima (Figure 2(a)), where the returns falling outside of the segment belonging to the main cluster were given a temporary classification according to which non-main segment they intersected with (Figure 2(b)).

In this process, a number of clusters of returns within the point cloud were reassigned with a temporary class value. These temporary classifications were then either assigned to an existing ITC cluster or were designated as a unique ITC classification. A temporary cluster was merged to an existing ITC classification using two approaches: (1) if the horizontal extent of either the ITC or the temporary class exceeded 50% overlap of horizontal area with each other (determined with convex hull), then the two classes were merged; or (2) the cluster's distance to neighboring classes was assessed and merged if the proximity was lower than a threshold value. When determining the ITC classification of a temporary cluster based on distance to neighbor, the number of an ITC's or temporary class' neighboring points within .5 m were then assessed. The class with the largest number of returns in this range was then assigned to the current temporary class. This process was repeated until changes to ITC delineation classifications were no longer made. Any temporary classifications that still existed after this process were then given a unique ITC classification. If an ITC object existed within a plot-level extent with a height of ≤2 m, it was considered understory and automatically excluded. A sample classification is presented in Figure 3.

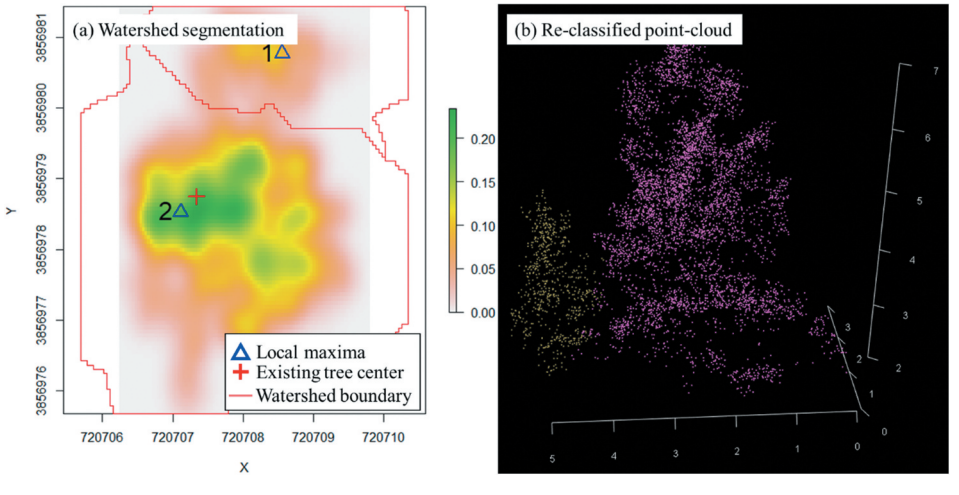

Figure 2. (a) A watershed segmentation applied to the 2D kernel density raster produced from the returns classified as part of the current ITC, with separate local maxima used as seed points. Returns were reclassified according to which regions they intersected with. (b) The returns which are part of the cluster of tree crowns were reclassified into two separate ITC objects.

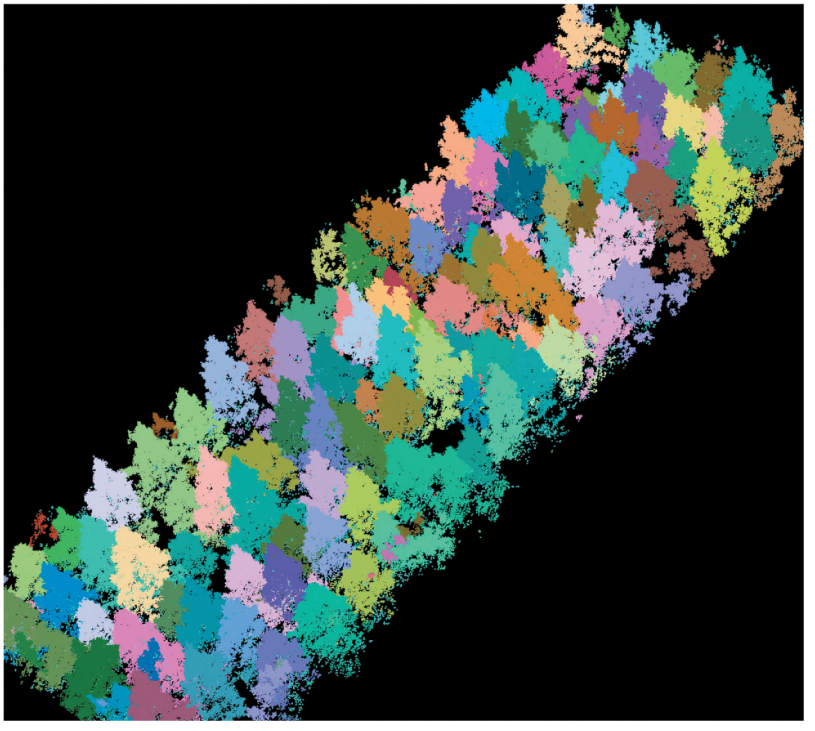

Figure 3. A sample classification for two neighboring field plot locations. Both plots had a stem spacing of 4.42 × 3.66 m, but were of a different genotype.

2.6. Individual-tree metric calculation

Any delineated ITC objects (as defined in Sections 2.4.4 and 2.5) which were outside the original field plot polygon extent were ignored. For the purpose of determining tree position, we assumed that the tallest DLS return from within each of the ITC delineations were on or near the location of the top of the tree, and directly above the tree stem, and that the stem was straight. The horizontal coordinates of this top return were then stored. The field recorded individual-tree GPS coordinates were therefore compared directly with the delineated ITC objects center-top locations derived from the DLS with the following approach. A 1 m buffer was applied to the planting location coordinates. This size was selected as it was smaller than the smallest planting density spacing (i.e. 1.4 × 3.6 m). ITC top location points existing within these extents were assessed. If there were multiple ITC top locations, the ITC top location closest to the planting location center was retained. Each planting location therefore had a paired ITC location for direct comparison. If a planting location was determined to be for a dead tree, and no ITC delineations were found in the proximity, it was excluded. This process was repeated for all eight pulse densities tested. The probability of an ITC being delineated in the correct location, given a specific pulse density, was assessed (more details are given in Section 2.8).

Each living tree was expected to have an associated ITC object. DLS-derived measurements were then compared directly to field height measurements. The largest return height for each ITC object was assumed to be the top height, for each of the pulse densities tested (Table 2).

Estimates of ITC crown diameter were made by first calculating an alpha-hull around the horizontal extent of the classified returns (>1 m height). This alpha-hull was then converted into a polygon and the largest uninterrupted distance from one side to the other was calculated. This distance served as the estimate of crown diameter and was compared to the largest field-measured crown diameter for that stem. Consequently, each tree was located with GPS coordinates and ITC coordinates and had corresponding field-measured and DLS-estimated heights and crown diameters.

2.7. DLS LAI calculation

Finally, we estimated plot-level DLS-derived LAI and compared it to field-derived LAI. Specifically, the estimates here are 'effective' LAI (eLAI). This eLAI assumes a simple random foliage distribution and also includes area covered by branches and stems (Stenberg 1996). For each of the 108 plots, we calculated a light penetration index based on vertical return count distribution using the above/below ratio index (ABRI); which, to our knowledge, is the best performing index (Sumnall et al. 2021):

$$ABRI = \frac{\sum^{R_{>T}}}{\sum^{R_{\leq T}}} \tag{2}$$

where R denotes an individual ALS return, and T represents a height threshold, of which returns are excluded if under or over this height. Here, T was set to 1 m above ground. As indicated in Zhao and Popescu (2009), the height threshold (T), at which indices are calculated, has a large influence on eLAI estimates. This height threshold is commonly set to be close to the field LAI2200 measurement height (Magnussen and Boudewyn 1998; Zhao and Popescu 2009; Sumnall et al. 2016). Model coefficients for estimating eLAI from ABRI were determined in Sumnall et al. (2021), where this approach produced an R^2 of .88 ($p < .001$) when regressing ABRI values against field LAI2200 measurements. Scan angle was limited to ≤15° in order to remove the uncertainty observed at large, off-nadir angles as in Liu et al. (2018).

2.8. Statistical analysis

Field- and DLS-derived values were directly compared at the individual-tree level (n = ~6804 individual-trees) for correctly located ITC locations and metrics concerning the matched planting location. Height and crown diameter estimates were assessed at the individual-tree level (n = ~2700 individual-trees). Comparisons of eLAI were at the plot-level (n = 108). All statistical analyses were conducted in R (v3.4; R Core Team 2021), with a significance alpha threshold of $p \leq .05$.

Student's t-test, as implemented in R (v3.4; R Core Team 2021), was used to directly compare the field and equivalent DLS derived values in order to determine if the means of two datasets were significantly different from each other. Root mean square error (RMSE) was used as a measure of the differences between values predicted from DLS and field measurements and is expressed as:

$$RMSE = \sqrt{\frac{\sum_{i=1}^{n} (x_i - y_i)^2}{n}} \tag{3}$$

where y are the predicted variables, x is the field measured variables, i is the individual-tree (ITC detection, top-height, and crown width) or plot (eLAI) value and n is the number of samples.

Standard error for a given metric was calculated as follows:

$$s = \sqrt{\frac{1}{n-2}\sum_{t=i}^{n} e_t^2} \tag{4}$$

where e is the error, i is a given observation of t, and n is the number of sample points. RMSE and standard error were computed at the site-level when comparing individual field and ITC delineation success (~6804 potential stems) and the estimates of height and crown diameter (~2700 potential stems). Estimates of eLAI were available at the field-plot level, where RMSE and standard error were computed for the 108 samples.

2.8.1. Mixed effect modeling for individual trees

We examined the influence of pulse density and planting density on estimation accuracy. The analysis of variance (ANOVA) for ITC delineation (0 = incorrect, 1 = correct, for all 6,804 potential stems) was assessed using the *glmer* function in the lme4 package (Bates et al. 2015) and included a binomial error distribution with a logit link. Pulse density (*Pulse*) and planting density (*Density*) were fixed effects. Plot (*PlotID*) nested within genotype (*Geno*) nested within silviculture (*Silv*) was the random effect. Which can be expressed as:

$$Tree = Density \times Pulse + \left(1 \middle| \frac{\frac{Silv}{Geno}}{PlotID}\right) \tag{5}$$

Post-hoc comparisons were made using the least squares means (LS means) function in the lsmeans package (Lenth 2016). The interaction between stem planting density and pulse density fixed effects was performed using the Anova function from the car package in R (Fox and Weisberg, 2019), where Chi-square statistics are reported.

2.8.2. Mixed effect modeling for metrics at the plot-level

Plot-level values of RMSE were computed from the ITC metrics: height and crown diameter, and their corresponding field values (n = 108). Plot-level RMSE was the dependent variable for these analyses. As there was a single estimated value for eLAI per plot, the differences in field- and DLS-derived values were calculated, hereafter referred to as eLAI difference (n = 108). Mixed-effects type III ANOVA, with Satterthwaite's method, of tree height and crown diameter RMSE and eLAI difference were fit using the lmer function in the lme4 package in R v.3.5 (Bates et al. 2015). P-values were calculated using the lsmeans function (lsmeans R package). Fixed and random effects were expressed as follows:

$$Height_{RMSE} = Density \times Pulse + \left(1 \middle| \frac{\frac{Silv}{Geno}}{PlotID}\right) \tag{6}$$

$$Crown_{RMSE} = Density \times Pulse + \left(1 | \frac{\frac{Silv}{Geno}}{PlotID}\right) \quad (7)$$

$$LAI_{diff} = Density \times Pulse + \left(1 | \frac{\frac{Silv}{Geno}}{PlotID}\right) \quad (8)$$

Where $Height_{RMSE}$ and $Crown_{RMSE}$ is the RMSE of ITC height and crown diameter calculated at the plot-level, respectively, and eLAI difference is LAI_{diff}. The interaction between fixed effects was evaluated using the anova function in R, where F statistics are reported.

3. Results

3.1. DLS metric estimation and pulse density

For all variable estimates, as pulse density decreased, mean DLS estimates of ITC counts, tree height, and crown width also decreased, with the exception of plot-level eLAI which remained relatively consistent (Table 3). With the exception of the plot-level eLAI estimates, all comparisons of DLS derived ITC metrics were significantly different from field values ($p < .05$). The success of the ITC delineation was highest in the low-density planting plots, and lowest in the high-density planting plots. As illustrated in Table 3, the estimates of mean tree height decreased in value when pulse density decreased relatively consistently. Estimates when compared with field values differed by .29 to 2.42 m, .18 to 2.65 m and −.02 to 2.44 m for low, medium and high planting density plots, respectively for pulse densities of 300 and .25 ppm^{-2}, respectively. DLS estimates of tree crown mean diameter for the high planting density planting plots were consistently less than those of the low planting density plots.

3.2. Correspondence of field and estimated tree positions

The overall uncertainty (RMSE) and correct mean are relatively consistent (Table S1, ±5% and ±3%, respectively) for pulse densities 300, 100, 50, 10 and 5 pulses m^{-2} at the individual tree level. As pulse density drops below 1 pulse m^{-2}, uncertainty increases. Stem planting density has a large impact on ITC delineation accuracy, as evident in Table S2 and in Figure 4 Within the same stem planting density, the percentage of correctly delineated ITCs was relatively consistent above a certain pulse density. For low-density planting, the largest percentage of stems were delineated correctly among planting densities (an average of ~87% when pulse density was ≥5 pulses m^{-2}). Medium planting density performed slightly poorer than the low planting density, with an average of ~70% of stems correctly delineated when pulse density was ≥1 pulses m^{-2}. The ITC delineation process performed the worst in high planting density plots, where an average of only ~50% of stems were correctly delineated when the pulse density was ≥.5 pulses m^{-2}. The amount of consistency of the RMSE for each of the stem densities differs. Specifically, the RMSE noticeably increases (see Figure 4) when pulse density decreases below 5 pulses m^{-2} for low planting density plots, whereas this decrease occurs at 1 pulse m^{-2} for medium planting density plots and .5 pulses m^{-2} for high planting density plots. There were no additional ITCs delineated within the field-plot extents which could not be paired with a field GPS location or were not classified as understory (<2 m), implying that there was no obvious commission error within the current study.

Table 3. Mean estimates for all measurements taken, both field- and DLS-derived. ITC is individual tree crown and its corresponding values are the number of trees located of a possible 63 at the plot-level. Tree top height is the top height of the canopy in meters. Crown diameter is the largest horizontal diameter of an individual tree crown in meters. eLAI is leaf area index (m^2 m^{-2}). Mean is calculated for all 36, 63-tree plots in a given stem planting density. Field is referring to field-derived estimates. The eight levels of pulse densities used are measured in pulses per square meter (pulses m^{-2}). Asterisks (*) denote values DLS derived estimates are statistically different (p <.05) from the field value, as determined by Student's t-Test.

Metric name	Trees ha^{-1}	Mean field value	Mean DLS estimates (pulses m^{-2})							
			300	100	50	10	5	1	0.5	0.25
ITC counts	618	53.14	53.14*	46.56*	42.53*	47.08*	46.61*	44.17*	39.17*	32.72*
	1236	53.72	37.14*	33.94*	37.86*	38.86*	39.17*	38.03*	34.25*	27.72*
	1854	53.69	25.64*	22.42*	25.61*	27.03*	27.03*	28.56*	28.50*	23.33*
Tree top height (m)	618	10.98	10.69*	10.62*	10.57*	10.16*	10.10*	9.38*	9.02*	8.56*
	1236	11.82	11.64*	11.58*	11.53*	11.09*	10.88*	10.13*	9.83*	9.17*
	1854	11.92	11.94*	11.95*	11.85*	11.49*	11.23*	10.44*	9.96*	9.48*
Tree crown diameter (m)	618	4.27	2.63*	2.33*	2.26*	1.70*	1.81*	0.97*	0.57*	0.23*
	1236	3.43	2.24*	1.98*	1.91*	1.41*	1.40*	0.72*	0.42*	0.16*
	1854	3.09	2.33*	2.11*	2.04*	1.49*	1.44*	0.73*	0.38*	0.16*
Plot eLAI	618	3.05	2.85	2.85	2.85	2.83	2.86	2.87	2.90	2.93
	1236	3.67	3.63	3.63	3.63	3.64	3.62	3.64	3.64	3.80
	1854	3.64	3.51	3.51	3.52	3.49	3.51	3.48	3.56	3.39

The main effects (pulse density: Chi squared = 798.94; p-value < .01; spacing: Chi squared = 451.26; p < .01) and interaction of stem planting density and pulse density were significant (Chi squared = 463.69; p < .05) in predicting ITC delineation. The probabilities in correctly delineating ITC crown with respect to pulse density and planting density is illustrated in Figure 5.

Across all planting densities, the general trend was to see decreasing RMSEs as pulse density increased. RMSEs tended to stabilize as pulse densities exceeded 5 pulses m^{-2} (Table S1, Figure 5). Pulse densities of 300, 100 and 50 pulses m^{-2} had similar ITC delineation probabilities (ranging 47 to 48%, p < .05). The pulse densities of 10 and 5 pulse m^{-2} share a similar probability value (50%), and the pulse densities of 1 and .5 pulses m^{-2} are likewise similar (53%).

For the results of pulse densities under the medium planting density tree planting, 14 of the 28 pairwise comparisons of pulse density were significantly different (p < .05). RMSE decreased until 5 pulses m^{-2} and then all higher pulse densities had similar values (ranging from 70 to 72%) with the exception of comparisons to 300 pulses m^{-2}, which was similar to 1 pulse m^{-2} (ranging from 69 to 71%).

In low planting density tree planting, 10 of the 28 pairwise comparisons of pulse density were not significant (p < .05). RMSE decreased from .25 to 5 pulses m^{-2} and then RMSE values were similar among pulse densities of 10 through 300 pulses m^{-2} (where values ranged from 87.6 to 88.5%).

For post hoc comparison of pulse densities irrespective of tree planting density, high pulse densities (300, 100, 50, 10, and 5 pulses m^{-2}) rarely differed significantly. The pulse densities of .25, .5, 1 and 5 pulses m^{-2} had sequentially increasing value ranges for detection probability. The remaining pulse densities (300 to 10 pulses m^{-2}) shared a similar value range (18.6 to 25.0%). At each individual pulse density, tree planting density RMSEs for ITC detection were significantly different with RMSEs in the order of higher density > medium density > low density (p < .01).

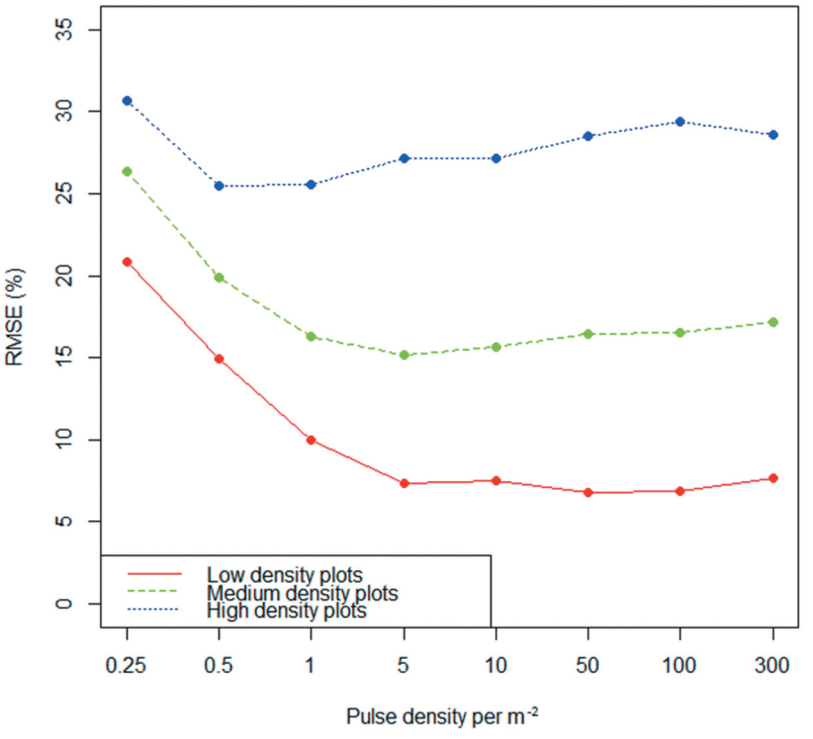

Figure 4. RMSE (%) for correctly delineated individual tree crowns (ITCs) calculated at the plot-level, i.E. DLS estimated tree tops within 1 m of a GPS planting location. Each line corresponds to a specific planting density: Low (618 trees per hectare (TPH)), medium (1236 TPH) and high (1854 TPH), respectively.

3.3. Estimation of tree top height

Across all planting densities, there was a general trend to have lower RMSE for top height estimated (the difference between field- and DLS-derived ITC estimates) as pulse density increased. RMSE and standard error stabilized at and above 50 pulses m^{-2} (Table S3). Top height RMSE in the high, medium and low-density tree plantings showed a decrease in RMSE from .5 to 50 pulses m^{-2} after which there was no significant change (Table S4).

There was a significant interaction between pulse density and planting density in predicting tree top height RMSE ($F = 7.79$; p-value < .01). In general, estimation accuracy for top height increased with decreasing tree planting density (Table S4 and Figure 6). For pulse densities of 300 and 50 pulses m^{-2}, the comparison between high and low, and high and medium stem density was significantly different. The differences in RMSE among stem densities at each of the eight pulse densities was small (±.2 m; Figure 6) but significant ($p < .05$). The estimates of RMSE for top height at a pulse density of .25 was similar >2.55 m (±.2) for all three stem densities.

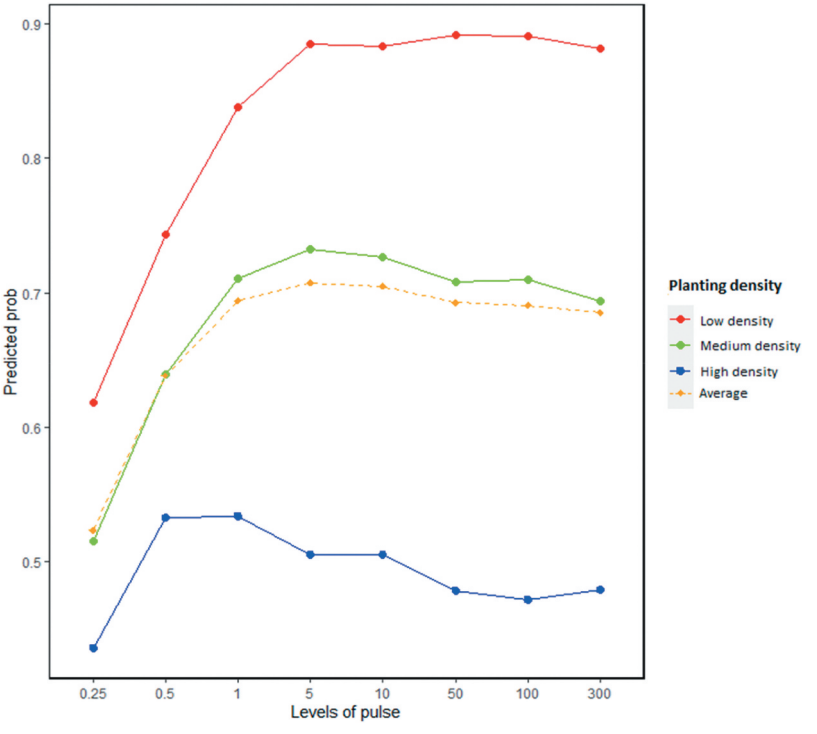

Figure 5. Post-Hoc least-squares means interaction plot illustrating the differences in probabilities in successful individual tree crown delineation for the three planting densities (Low = 618 trees per hectare (TPH), Medium = 1236 TPH, and High = 1854 TPH) and pulse densities (pulses m^{-2}).

3.4. Estimation of individual tree crown horizontal diameter

Crown diameter at the individual tree level was underestimated by DLS across all planting densities (Figure 7). Overall, as pulse density decreased, there was a corresponding increase in RMSE and standard error (Table S5). The largest overall RMSE was observed for ITCs located in low-density planting plots. The smallest overall RMSE for ITCs was observed in the high-density planting plots (Table S6). The RMSE decreased for all planting densities as pulse density increased, with similar slopes among planting densities but respective intercepts (Figure 8). The differences of crown diameter among densities were slightly more pronounced as pulse density decreased, however. The difference between crown diameter RMSE at a pulse density of 300 pulses m^{-2} was .65 m when comparing high to low density planting, whereas for a pulse density of .25 pulses m^{-2}, the RMSE was 1.24 m between high to low density planting.

At the plot level, the interaction of pulse density and stem planting density was significant in explaining field plot-level crown diameter RMSE ($F = 11.8$; p-value $< .01$). The effects of varied pulse densities were identical across all three planting densities with

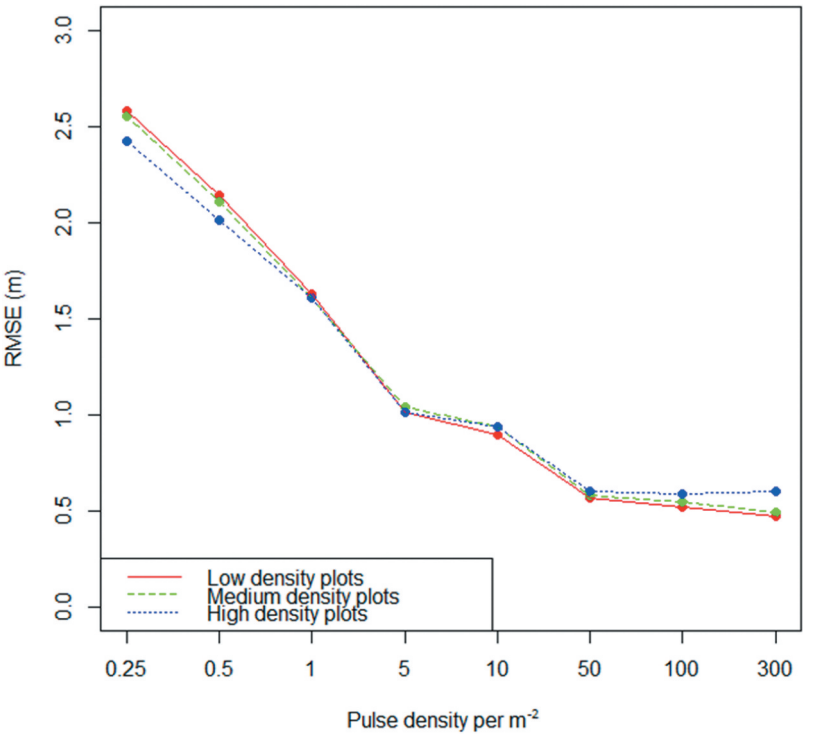

Figure 6. RMSE (m) for top height for all ITCs, and colored according to stem planting density: Low (618 trees per hectare (TPH)), Medium (1236 TPH) and High (1854 TPH) planting densities, respectively.

accuracy generally declining with decreasing pulse density. Crown diameter RMSE values among the three planting densities and within each of the eight pulse densities were all significantly different ($p < .05$; Figure 8).

3.5. Estimation of plot-level leaf area index

At the field plot level, the interaction of pulse density and stem planting density was significant in predicting eLAI difference ($F = 2.1$; p-value $< .05$). The difference between DLS- and field-measured eLAI was relatively similar across all pulse densities (Table S7), until pulse density dropped below 1 pulse m^{-2}.

RMSE values were relatively consistent for all three stem densities when pulse density was or exceeded .5 pulses m^{-2} (Table S8 and Figure 9). Low planting density plots had a consistently higher RMSE for all pulse densities among the three planting densities. The eLAI RMSE values for .25 pulses m^{-2} under high planting density plots was greater than all the other pulse density values. Medium planting density plots had the lowest overall RMSE at each pulse density (except at .25 pulses m^{-2}) among the planting density plots.

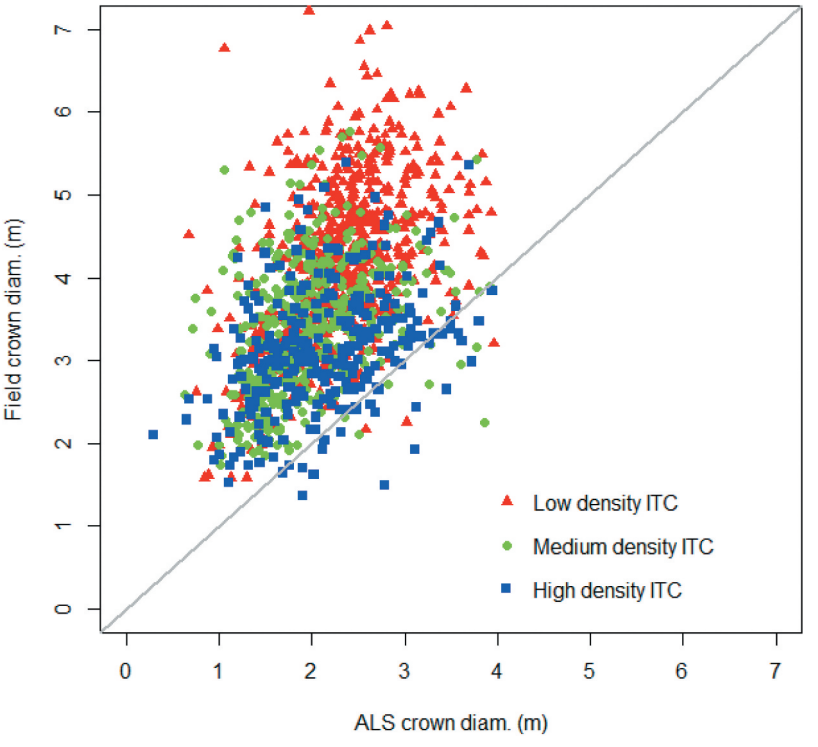

Figure 7. Comparison of paired field and ITC diameters for metrics generated at a pulse density of 300 pulses m^{-2}, colored by stem planting density: Low (618 trees per hectare (TPH)), Medium (1236 TPH) and High (1854 TPH) planting densities, respectively. The solid-gray denotes a 1:1 relationship.

Under high planting density, only .5 and .25 pulses m^{-2} differed significantly, with the .5 pulses m^{-2} having a lower RMSE (Table S8). For medium-density tree planting, only 1 pulse m^{-2} showed lower RMSE than other pulse densities. Finally, for low-density tree plantings, there was no effect of pulse density on RMSE.

4. Discussion

4.1. Accuracy of individual tree crown delineation

The accuracy of the ITC delineation was strongly dependent on planting density. The largest proportion (~88%) of delineated ITCs that corresponded to field GPS coordinates were observed within plots that had the lowest stem planting density. ITC delineation was ~71% for medium planting density, and ~49% for high planting density (~49%) when pulse density was ≥5 pulses m^{-2}.

ITC RMSE within the three stem densities tested was relatively consistent (±3%) for pulse densities ≥5 pulses m^{-2}. This similarity in detection accuracy within a planting density implies that the planting density was a more important consideration than pulse density. Differences in RMSE among planting densities could be as high as ~40% between low to high density planting. This finding is in agreement with those of Kaartinen et al. (2012). Greater crown overlaps in high planting densities likely resulted in a reduction in

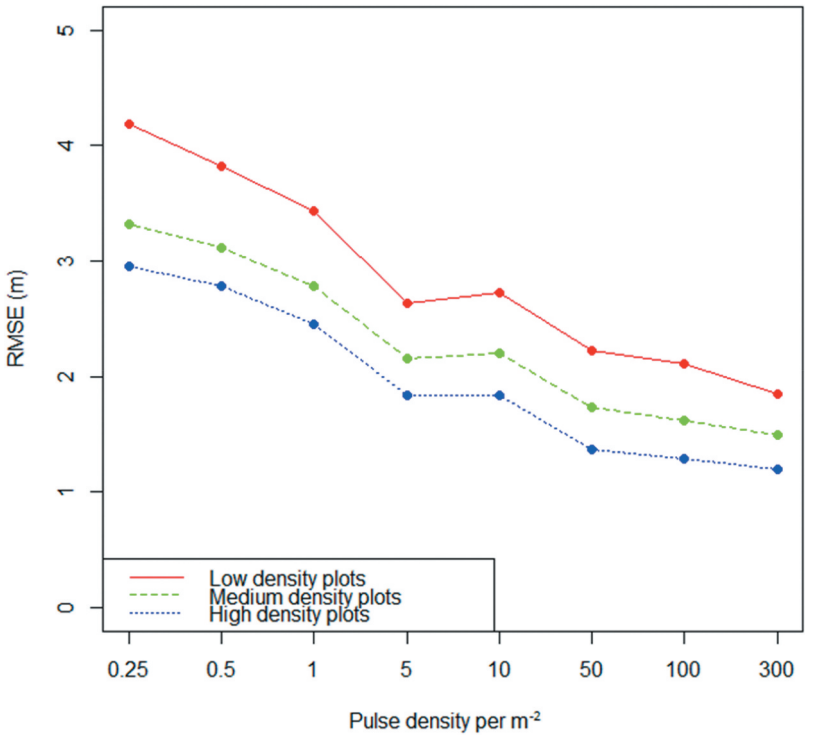

Figure 8. RMSE (m) for crown diameter for all plots, separated into low (618 trees per hectare (TPH)), Medium (1236 TPH) and High (1854 TPH) planting density plots, respectively.

physical features in the point cloud surface which complicated ITC delineation using the current method. As with some other methods (e.g. spatial wavelet analysis and variable window filters; Falkowski et al. 2008), some tree crowns in this study may have been too close together or suppressed to be accurately delineated.

The underestimation of stems using ITC delineation methodologies is a common phenomenon. Our values fell within previously reported detection rates which range between 25 to 102%, 72% (>200 to <400 TPH), 86% (500 m^2 plots with 9 to 35 stems), and 70–90% (<500 TPH) (Kaartinen et al. 2012; Jakubowski et al. 2013b; Li et al. 2012; Wang et al. 2016, respectively).

Across all planting densities, ITCs could generally be delineated consistently at pulse densities above 5 pulse m^{-2} for the site used in this study. However, when pulse densities decreased below 5 pulse m^{-2} the probability of correctly delineating ITCs decreased significantly. The differences in the distributions of pulses at lower pulse densities may have resulted in differences in ITC center positions and horizontal extents, or, more specifically, the ITCs may have been omitted as pulse density decreased below 5 pulses m^{-2}.

As no commission error (false positives) was observed, we conclude that some ITC objects occasionally represent a cluster of multiple tree crowns, resulting in omission error (false negatives). A potential method that could be used to separate overlapping tree crowns is the adaptive mean-shift algorithm (Ferraz et al. 2012) which demonstrated the capability to classify the point-cloud into ITCs based on the distribution of all returns,

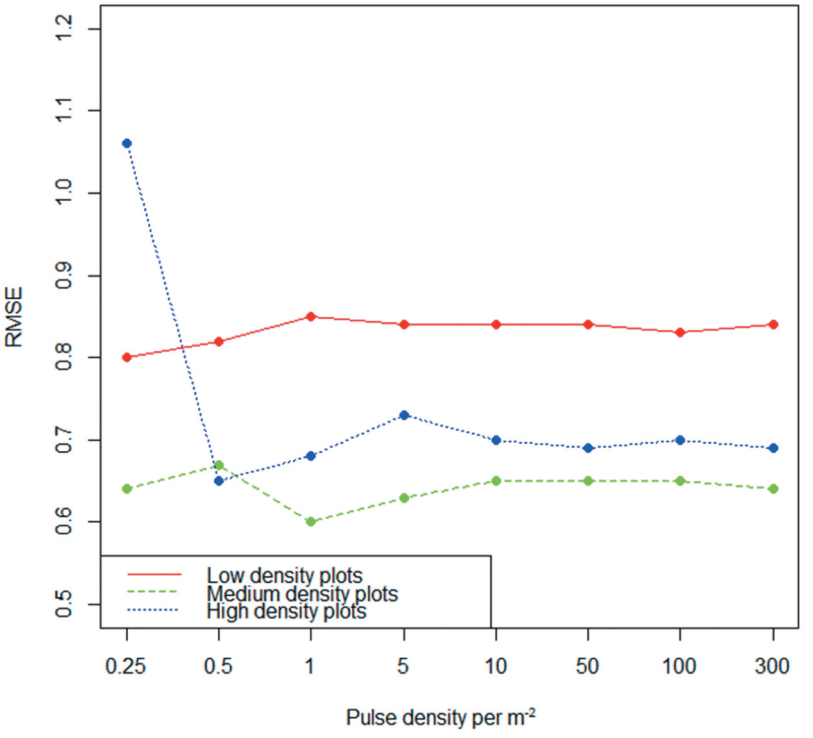

Figure 9. RMSE of plot-level leaf area index (m^2 m^{-2}) for all plots separated into low (618 trees per hectare (TPH)), Medium (1236 TPH) and High (1854 TPH) planting density plots, respectively.

rather than just the top surface returns. This approach could classify ITCs in both the over- and understory, however, a bandwidth (or search area) must be set and an incorrect bandwidth size can result in misclassification. Ferraz et al. (2016) utilized regionally specific allometry to determine bandwidth. Alternatively, Yan et al. (2020) proposed a method to automatically determine bandwidth from canopy height for a plantation forest which resulted in correctly delineating between 80% and 95% of crowns. With the availability of high pulse density datasets which conceivably allow more returns from features below the canopy (Silva et al. 2017), in addition to the inclusion of high scan angles which potentially allow returns from individual tree stems (Corte et al. 2020), parts of the individual tree stems may be available in the point-cloud. Therefore, existing methods developed for stem classification used in terrestrial laser scanning, such as a Hough Transform circle search algorithm (de Conto et al. 2017), may be implemented to detect clusters of trees. Accurate tree delineation is critical to further estimate tree top height and crown diameter.

4.2. Estimation of tree top height

In general, higher pulse densities increased accuracy of tree top height estimation under all planting stem densities, but ≥50 pulses m^{-2} did not provide additional benefit. Planting density showed small effects on top height RMSE (±.2 m). Top height estimate comparisons of the different planting densities within each pulse density indicated top height estimates were consistent with one another across planting densities.

The results in the current research for ITC-derived height RMSE at high pulse densities (.5 m ± .1 m) were slightly larger than the previously reported RMSEs of .31 m in pure and mixed *Eucalyptus* spp. and maritime pine plantation forests in Portugal at 9.5 pulses m^{-2} (Ferraz et al. 2012). However, the crown shape/structure of *Eucalyptus* spp., which made up the majority of the trees in that study, is substantially different than loblolly pine. When examining ITC implementations in conifer-dominated forests, the comparison was more favorable, where RMSEs ranged from .77 to 4.27 m (Falkowski et al. 2006; Lee and Lucas 2007; Jakubowski et al. 2013b).

Underestimation of top heights using LiDAR has been reported. Popescu and Zhao (2008) reported an underestimation in top height for both coniferous and deciduous forests, which required the use of a correction calculated through statistical analysis (in the range of 1.22 to 2.04 m). Likewise, Leckie et al. (2003) reported a similar issue of underestimating tree height, with an average error of 1.3 m, for Douglas-fir dominated forests in British Columbia, Canada, and suggested an insufficient amount of energy might have been returned from the very top of the tree from a laser pulse for detection. For the current study, the uncertainty was more prevalent as pulse density decreased. As pulse density decreased, mean height estimates decreased. This finding supports the assumption that detection of tree top height was dependent on DLS pulses returning energy from the top of the tree.

4.3. Estimation of individual tree crown horizontal diameter

As with other metrics, the accuracy of crown diameter estimates decreased with decreasing pulse density. The highest accuracy was for 300 pulses m^{-2}, however, DLS-derived crown diameters were generally smaller than field-based estimates of crown diameters. The reduction in estimated crown diameter size as pulse density decreased implies that lower pulse densities were potentially missing parts of tree crowns due to reduced sampling. When stratifying by stem density, the increase in RMSE as pulse density decreased was almost constant between the three planting densities, just with a different intercept. At lower pulse densities, the separation of RMSE values by planting density was greater. The lowest error in crown diameter estimates was consistently observed for high planting density plots while the largest error was observed for the low-density. It should be noted that the field measured crown sizes were variable (with means between 3.1 and 4.3 m). Observed error in the DLS-estimates tended to increase with increasing crown size. This result was potentially related to greater variability existing among larger objects.

As noted before, much of the literature which reports crown diameter typically uses a CHM or other raster imagery for the delineation of ITC objects (Falkowski et al. 2006, 2008; Popescu and Zhao 2008). Previous studies reported RMSE values between 1.35 and 2.08 m. This was similar to our RMSE values, which ranged from 1.20 to 1.85 m (300 pulses m^{-2}) to 1.37 to 2.22 m (50 pulses m^{-2}).

Given the uncertainty observed in estimates of crown size, regardless of planting density, we conclude that parts of the crown may be missed or incorrectly classified. The merging and obscuring of crowns, for example, or a decreased probability of DLS returning from the edges of crowns, could potentially explain these sources of underestimation. As noted in Yáñez, Seiler and Fox (2017), these different genotypes exhibited differences in crown structural characteristics, such as leaf area, which may have contributed to additional uncertainty to correctly delineating all stems in an area. Similarly, Jakubowski, Guo and Kelly (2013a) state that metrics related to coverage (e.g. canopy cover) were sensitive to pulse densities, particularly as pulse density decreases below 20 pulses m^{-2}. The field measurement protocol used here, i.e. within and between planting rows, may not have had extended along the axis of the widest spacing in all cases, and may represent an additional source of uncertainty. Goodwin, Coops and Culvenor (2006) demonstrated there was a relationship between increases in distance from the sensor (and, by extension, laser footprint size) and the accuracy of crown area estimates. The authors hypothesized that less light energy is returned to the sensor resulting in a reduction of the number of returns recorded. With the small footprint sizes (~20 cm), and potentially small branch end objects in the context of the current study, a potential explanation would be that these ends are either missed or an insufficient amount of energy is returned from this part of the crown.

4.4. Estimation of plot-level effective leaf area index

The plot-level eLAI method used here appears relatively stable across pulse densities greater than .5 pulses $^{-2}$. This finding additionally supports that eLAI estimates may be stable among acquisition types as the eLAI estimation method was originally developed for conventional ALS (Sumnall et al. 2021). Accuracy was lowest in low planting density plots and, surprisingly, highest in the medium planting density plots. Estimates of eLAI RMSE were relatively consistent across pulse densities ≥.5 pulses m^{-2} (±.2) and within each planting densities (±.1). The largest RMSE was observed for high stem density and a pulse density of .25 pulses m^{-2}, which is a likely due to sampling error due to very few returns. This could be erroneous or a problem caused by a reduction in plot size (as suggested in Frazer et al. 2011). We conclude, however, that above the pulse density equal to or above .5 pulses m^{-2}, eLAI can be estimated accurately.

The RMSE eLAI values in the current study ranged from .64 to .84 at 300 pulses m^{-2} and were somewhat higher than other reported values of .47 (Sumnall et al. 2021), .45 to .67 for loblolly pine plantations (Peduzzi et al. 2012) or .29 to .38 for mixed woodlands (Zhao and Popescu 2009), or .32 to .36 for *Picea abies* (Solberg et al. 2009). Each of the examples noted here was produced using ALS. This difference, we conclude, was related to the difference in the method of acquisition or the influence of field plot size (Frazer et al. 2011). As noted previously, scan angles were constrained for eLAI estimates in order to avoid the problems outlined in Liu et al. (2018). This restriction may have the unintended

consequence of only sampling portions of field plots due to the UAV's flying altitude. Incomplete plot coverage may be responsible for the increased uncertainty. This result may have implications in using low altitude DLS for eLAI assessment.

4.5. Considerations and future work

We explored the use of DLS data to test a method of delineating ITCs directly from the point cloud. The use of DLS allowed for the analysis of a very high pulse density (300 pulses m^2). This was partially due to the use of all returns from scan angles 0 to 60°, a range uncommon in ALS acquisitions. Previous research has demonstrated that regressing a field plot-variable to an ALS derived point cloud summary metric was very sensitive to the scan angles used (Liu et al. 2018). Conceivably only part of an ITC may be returned from when scan angles are off-nadir within a single flight, where parts of the crown may be occluded from the sensor. This may have been an issue near the outer extent of the current study's plots. Holmgren, Nilsson and Olsson (2003), when exploring the influence of scan angle at the plot scale, observed that off-nadir angles yielded slightly more canopy returns. Leite et al. (2020) found significant differences ($p < .05$) from airborne LiDAR to field-measured tree heights at nadir scan angles (0–7°). Given that no statistical models were used in the delineation of ITCs, instead the methods here were dependent on the exterior returns of the point cloud and local relative 3D density, we would argue that this issue does not apply in this context. The inclusion of high scan angles, may allow for an increased number of crown exterior returns (Holmgren, Nilsson and Olsson 2003) and returns from additional features such as the sides of the tree stems (Corte et al. 2020). For the estimation of plot-level eLAI, however, the scan angle range was constrained.

Plot-level metrics can be calculated with relatively low pulse densities. As noted by Kamoske et al. (2019), only very low pulse densities can impact the estimates of forest structural characteristics at the plot-scale, although higher densities were considered more reliable (>20 pulses m^{-2}; Shao et al. 2019). The results at the individual tree-scale in the current research may suggest that the size of the object being considered for analysis will impact this assumption. There was evidence to suggest sensor-induced bias can also influence estimate accuracy (Shao et al. 2019). Kamoske et al. (2019) noted that different sensors can have different canopy penetration capabilities, where beam divergence and pulse repetition frequency can determine the quality of the point cloud. Differences in acquisition characteristics, particularly from different sensor designs, will yield different distributions of returns in the point cloud for the same location (e.g. Kamoske et al. 2019; Yu et al. 2020). Future work would therefore need to evaluate the impact of different acquisition characteristics, for example from different sensors, on estimate accuracy.

The effect of laser footprint size on estimates such as height accuracy has received little attention in the literature. Andersen, Reutebuch and McGaughey (2006) and Roussel et al. (2017) found a similar effect of underestimating tree height, which increased as laser footprint size increases. Different accuracies were also observed for height estimates among different tree species (specifically: ponderosa pine and Douglas-fir) when considering footprint size It is possible the size and spatial-arrangement of the object being scanned will influence estimate accuracy.

Platform altitude, laser power and footprint size can potentially reduce the intensity of laser beam incident on a given surface area, thus decreasing the probability of recording a last return above the noise threshold (Goodwin, Coops and Culvenor 2006). Given DLStechnology is relatively new, lack of standardization suggests that acquisition specific considerations may be a source of uncertainty. Likewise, we used ground-based measurements as our standard in this analysis. There was error associated with field measurements from the ground not explored here.

We artificially decimated the DLS point cloud using GPS time to achieve the different pulse densities. This could conceivably yield different results than actual unique acquisitions with a different initial pulse density. Furthermore, the results from a systematic decimation approach would differ from a random one, were non-uniform pulse densities would be possible, and therefore yield different results.

It should be noted that the study site used here potentially differs to typical operational forest sites, in terms of size, homogeneity and spatial arrangement. Again, future work would be necessary to evaluate these methods in different environmental contexts.

Our results suggest that relatively low pulse density DLS data may be capable of estimating individual canopy structural features and plot-level eLAI metrics reliably in most situations. Increased pulse density appears to increase estimate accuracy of most metrics, but only to a point. Tree size and their proximity to each other were also determining factors of accuracy. The results here provide practical guidance for forest managers who will make decisions concerning the tradeoff of data quality and coverage against cost when planning new DLS or ALS acquisitions.

5. Conclusions

The tradeoff the exists between data quality, spatial coverage and cost when planning new LiDAR acquisitions is a critical one for forest managers to consider. The results demonstrate the potential of DLS to provide data at various levels of accuracy as determined by varied pulse densities. For individual tree delineation, accuracy was relatively consistent, and only decreased at low pulse densities (≤5 pulses m^{-2}). When considering the ITC-scale, however, estimates appeared to be more sensitive to pulse density, as higher pulse densities generally produced greater accuracy, but only up to a point. Usually pulse densities >50 pulses m^{-2} did not result in much greater accuracy but some features may not be captured at lower pulse densities (≤10 pulses m^{-2}). As one of the main limitations to accurate forest metric estimation is ITC delineation, improved methods to separate clustered crowns would be beneficial.

Research highlights

- LiDAR pulse density and stem planting density influence individual tree crown delineation;
- Individual-tree-level estimates are more sensitive to pulse density than plot-level estimates;
- Above a pulse density of 0.5 pulses m^{-2} LAI can be estimated with consistent accuracy;
- Higher pulse densities provided higher accuracy for individual-tree estimates.

Disclosure statement

No potential conflict of interest was reported by the author(s).

Funding

This work was primarily funded by the Forest Productivity Cooperative. This work was also supported by the Virginia Agricultural Experiment Station (Critz, Virginia), and the USDA National Institute of Food and Agriculture, U.S. Department of Agriculture (Washington, DC, USA).

Data availability statement

Data available on request from the authors. The data that support the findings of this study are available from the corresponding author, MJS, upon reasonable request.

References

Almeida, D. R. A. D., S. C. Stark, G. Shao, J. Schietti, B. W. Nelson, C. A. Silva, E. B. Gorgens, R. Valbuena, D. D. A. Papa, and P. H. S. Brancalion. 2019. "Optimizing the Remote Detection of Tropical Rainforest Structure with Airborne Lidar: Leaf Area Profile Sensitivity to Pulse Density and Spatial Sampling." *Remote Sensing* 11 (1): 92. doi:10.3390/rs11010092.

Alonzo, M., B., Bookhagen, J.P. McFadden, A. Sun, and D.A. Roberts. 2015. "Mapping urban forest leaf area index with airborne lidar using penetration metrics and allometry." *Remote Sensing of Environment* 162: 141–153.

Andersen, H. E., S. E. Reutebuch, and R. J. McGaughey. 2006. "A Rigorous Assessment of Tree Height Measurements Obtained Using Airborne Lidar and Conventional Field Methods." *Canadian Journal of Remote Sensing* 32 (5): 355–366. doi:10.5589/m06-030.

Barilotti, A., S. Turco, and G. Alberti, 2006, February. LAI Determination in Forestry Ecosystem by Lidar Data Analysis. In: *Proceedings of Workshop 3D Remote Sensing in Forestry, Vienna, Austria*. Vol. 1415.

Bates, D., M. Mächler, B. Bolker, and S. Walker. 2014. "Fitting linear mixed-effects models using lme4." arXiv preprint arXiv:2014.5823.

Bivand, R., and C. Rundel. 2021. rgeos: Interface to Geometry Engine - Open Source ('GEOS'). https://CRAN.R-project.org/package=rgeos

Bivand, R.S., E. Pebesma, and V. Gómez-Rubio. 2013. *Applied Spatial Data Analysis with R*. Vol.10. Springer Science & Business Media.

Bivand, R., T. Keitt, and B. Rowlingson. 2021. rgdal: Bindings for the 'Geospatial' Data Abstraction Library. R package

Brandtberg, T., T. A. Warner, R. E. Landenberger, and J. B. Mcgraw. 2003. "Detection and Analysis of Individual Leaf-off Tree Crowns in Small Footprint, High Sampling Density LiDar Data from the Eastern Deciduous Forest in North-America." *Remote Sensing of Environment* 85 (3): 290–303. doi:10.1016/S0034-4257(03)00008-7.

Cannell, M. G. R. 1989. "Physiological Basis of Wood Production: A Review." Scandinavian Journal of Forest Research 4 (1–4): 459–490. doi:10.1080/02827588909382582.

Chen, J. M. and T. A. Black. 1992. "Defining Leaf Area Index for Non-Flat Leaves." *Plant, Cell & Environment* 15 (4): 421–429. doi:10.1111/j.1365-3040.1992.tb00992.x.

Corte, D. A. P., F. E. Rex, D. R. A. D. Almeida, C. R. Sanquetta, C. A. Silva, M. M. Moura, and B. Wilkinson et al. 2020. "Measuring Individual Tree Diameter and Height Using GatorEye High-Density UAV-Lidar in an Integrated Crop-Livestock-Forest System." *Remote Sensing* 12 (5): 863. doi:10.3390/rs12050863.

de Conto, T., K. Olofsson, E. B. Görgens, L. C. E. Rodriguez, and G. Almeida. 2017. "Performance of Stem Denoising and Stem Modelling Algorithms on Single Tree Point Clouds from Terrestrial Laser Scanning." *Computers and Electronics in Agriculture* 143: 165–176. doi:10.1016/j.compag.2017.10.019.

Eysn, L., M. Hollaus, E. Lindberg, F. Berger, J. M. Monnet, M. Dalponte, and M. Kobal et al. 2015. "A Benchmark of Lidar-Based Single Tree Detection Methods Using Heterogeneous Forest Data from the Alpine Space." *Forests* 6 (5): 1721–1747. doi:10.3390/f6051721.

Falkowski, M. J., A. M. Smith, A. T. Hudak, P. E. Gessler, L. A. Vierling, and N. L. Crookston. 2006. "Automated Estimation of Individual Conifer Tree Height and Crown Diameter via Two-Dimensional Spatial Wavelet Analysis of LiDar Data." *Canadian Journal of Remote Sensing* 32 (2): 153–161. doi:10.5589/m06-005.

Falkowski, M. J., A. M. Smith, P. E. Gessler, A. T. Hudak, L. A. Vierling, and J. S. Evans. 2008. "The Influence of Conifer Forest Canopy Cover on the Accuracy of Two Individual Tree Measurement Algorithms Using LiDar Data." *Canadian Journal of Remote Sensing* 34 (S2): S338–S350. doi:10.5589/m08-055.

Fekety, P. A., M. J. Falkowski, A. T. Hudak, T. B. Jain, and J. S. Evans. 2018. "Transferability of Lidar-Derived Basal Area and Stem Density Models Within a Northern Idaho Ecoregion." *Canadian Journal of Remote Sensing* 44 (2): 131–143. doi:10.1080/07038992.2018.1461557.

Ferraz, A., F. Bretar, S. Jacquemoud, G. Gonçalves, L. Pereira, M. Tomé, and P. Soares. 2012. "3-D Mapping of a Multi-Layered Mediterranean Forest Using ALS Data." *Remote Sensing of Environment* 121: 210–223. doi:10.1016/j.rse.2012.01.020.

Ferraz, A., S. Saatchi, C. Mallet, and V. Meyer. 2016. "Lidar Detection of Individual Tree Size in Tropical Forests." *Remote Sensing of Environment* 183: 318–333. doi:10.1016/j.rse.2016.05.028.

Fox, J., and S. Weisberg. 2018. *An R companion to applied regression*. Sage publications.

Frazer, G. W., S. Magnussen, M. A. Wulder, and K. O. Niemann. 2011. "Simulated Impact of Sample Plot Size and Co-Registration Error on the Accuracy and Uncertainty of LiDar-Derived Estimates of Forest Stand Biomass." *Remote Sensing of Environment* 115 (2): 636–649. doi:10.1016/j.rse.2010.10.008.

Gitelson, A. A., Y. J. Kaufman, R. Stark, and D. Rundquist. 2002. "Novel Algorithms for Remote Estimation of Vegetation Fraction." *Remote Sensing of Environment* 80 (1): 76–87. doi:10.1016/S0034-4257(01)00289-9.

Goodwin, N. R., N. C. Coops, and D. S. Culvenor. 2006. "Assessment of Forest Structure with Airborne LiDar and the Effects of Platform Altitude." *Remote Sensing of Environment* 103 (2): 140–152. doi:10.1016/j.rse.2006.03.003.

Hahsler, M., M. Piekenbrock, and D. Doran. 2019. "Dbscan: Fast Density-Based Clustering with R." *Journal of Statistical Software* 91 (1): 1–30. doi:10.18637/jss.v091.i01.

Heiskanen, J., L. Korhonen, J. Hietanen, and P.K. Pellikka. 2015. "Use of airborne lidar for estimating canopy gap fraction and leaf area index of tropical montane forests." *International Journal of Remote Sensing* 36 (10): 2569–2583. doi:10.1080/01431161.2015.1041177.

Hijmans, R. J. 2020. "Raster: Geographic Data Analysis and Modeling. R Package Version 3.4-5." https://cran.r-project.org/web/packages/raster/index.html

Holmgren, J., M. Nilsson, and H. Olsson. 2003. "Simulating the Effects of Lidar Scanning Angle for Estimation of Mean Tree Height and Canopy Closure." *Canadian Journal of Remote Sensing* 29 (5): 623–632. doi:10.5589/m03-030.

Hopkinson, C. and L. Chasmer. 2009. "Testing Lidar Models of Fractional Cover Across Multiple Forest Ecozones." *Remote Sensing of Environment* 113 (1): 275–288. doi:10.1016/j.rse.2008.09.012.

Hothorn, T., F. Bretz, and P. Westfall. 2008. "Simultaneous inference in general parametric models." *Biometrical Journal: Journal of Mathematical Methods in Biosciences* 50 (3): 346–363.

Hummel, S., A. T. Hudak, E. H. Uebler, M. J. Falkowski, and K. A. Megown. 2011. "A Comparison of Accuracy and Cost of LiDar versus Stand Exam Data for Landscape Management on the Malheur National Forest." *Journal of Forestry* 109 (5): 267–273.

Isenburg, M. 2019. "Lastools."[Online]. Accessed 3October 2019. https://rapidlasso.com/lastools/

Jakubowski, M. K., Q. Guo, and M. Kelly. 2013a. "Tradeoffs Between Lidar Pulse Density and Forest Measurement Accuracy." *Remote Sensing of Environment* 130: 245–253. doi:10.1016/j.rse.2012.11.024.

Jakubowski, M. K., W. Li, Q. Guo, and M. Kelly. 2013b. "Delineating Individual Trees from LiDar Data: A Comparison of Vector-and Raster-Based Segmentation Approaches." *Remote Sensing* 5 (9): 4163–4186. doi:10.3390/rs5094163.

Jeronimo, S. M., V. R. Kane, D. J. Churchill, R. J. McGaughey, and J. F. Franklin. 2018. "Applying LiDar Individual Tree Detection to Management of Structurally Diverse Forest Landscapes." *Journal of Forestry* 116 (4): 336–346. doi:10.1093/jofore/fvy023.

Jing, L., B. Hu, T. Noland, and J. Li. 2012. "An Individual Tree Crown Delineation Method Based on Multi-Scale Segmentation of Imagery." *ISPRS Journal of Photogrammetry and Remote Sensing* 70: 88–98. doi:10.1016/j.isprsjprs.2012.04.003.

Kaartinen, H., J. Hyyppa, X. W. Yu, M. Vastaranta, H. Hyyppa, A. Kukko, and M. Holopainen et al. 2012. "An International Comparison of Individual Tree Detection and Extraction Using Airborne Laser Scanning." *Remote Sensing* 4 (4): 950–974. doi:10.3390/rs4040950.

Kamoske, A. G., K. M. Dahlin, S. C. Stark, and S. P. Serbin. 2019. "Leaf Area Density from Airborne Lidar: Comparing Sensors and Resolutions in a Temperate Broadleaf Forest Ecosystem." *Forest Ecology and Management* 433: 364–375. doi:10.1016/j.foreco.2018.11.017.

Kato, A., L.M. Moskal, P. Schiess, M.E. Swanson, D. Calhoun, and W. Stuetzle. 2009. "Capturing tree crown formation through implicit surface reconstruction using airborne lidar data." *Remote Sensing of Environment* 113 (6): 1148–1162. doi:10.1016/j.rse.2009.02.010.

Kobayashi, H., Y. Ryu, D. B. Baldocchi, J. M. Welles, and J. M. Norman. 2013. "On the Correct Estimation of Gap Fraction: How to Remove Scattered Radiation in Gap Fraction Measurements?" *Agricultural and Forest Meteorology* 174–175: 170–183. doi:10.1016/j.agrformet.2013.02.013.

Kuznetsova, A., Brockhoff, P.B., and Christensen, R.H., 2017. lmerTest package: tests in linear mixed effects models. Journal of statistical software 82 (1): 1–26.

Kwak, D. A., W. K. Lee, J. H. Lee, G. S. Biging, and P. Gong. 2007. "Detection of Individual Trees and Estimation of Tree Height Using LiDar Data." *Journal of Forest Research* 12 (6): 425–434. doi:10.1007/s10310-007-0041-9.

Latifi, H. and B. Koch. 2012. "Evaluation of Most Similar Neighbour and Random Forest Methods for Imputing Forest Inventory Variables Using Data from Target and Auxiliary Stands." *International Journal of Remote Sensing* 33 (21): 6668–6694. doi:10.1080/01431161.2012.693969.

Leckie, D., F. Gougeon, D. Hill, R. Quinn, L. Armstrong, and R. Shreenan. 2003. "Combined High-Density LiDar and Multispectral Imagery for Individual Tree Crown Analysis." *Canadian Journal of Remote Sensing* 29 (5): 633–649. doi:10.5589/m03-024.

Lee, A. C. and R. M. Lucas. 2007. "A LiDar-Derived Canopy Density Model for Tree Stem and Crown Mapping in Australian Forests." *Remote Sensing of Environment* 111 (4): 493–518. doi:10.1016/j.rse.2007.04.018.

Lefsky, M. A., W. B. Cohen, G. G. Parker, and D. J. Harding. 2002. "LiDar Remote Sensing for Ecosystem Studies." *Bioscience* 52 (1): 19–30. doi:10.1641/0006-3568(2002)052[0019:LRSFES]2.0.CO;2.

Leite, R. V., C. H. D. Amaral, R. D. P. Pires, C. A. Silva, C. P. B. Soares, R. P. Macedo, A. A. L. D. Silva, E. N. Broadbent, M. Mohan, and H. G. Leite. 2020. "Estimating Stem Volume in Eucalyptus Plantations Using Airborne LiDar: A Comparison of Area-and Individual Tree-Based Approaches." *Remote Sensing* 12 (9): 1513. doi:10.3390/rs12091513.

Lenth, R.V. 2016. "Least-squares means: the R package lsmeans." *Journal of statistical software* 69 (1): 1–33.

LI-COR. 2012. "LAI2200 Instruction Manual." Accessed 1 November 2019. https://www.licor.com/env/support/LAI-2200C/manuals.html

Li, W., Q. Guo, M. K. Jakubowski, and M. Kelly. 2012. "A New Method for Segmenting Individual Trees from the Lidar Point Cloud." *Photogrammetric Engineering & Remote Sensing* 78 (1): 75–84. doi:10.14358/PERS.78.1.75.

Lin, Y., J. Hyyppä, and A. Jaakkola. 2011. "Mini-UAV-Borne LIDAR for Fine-Scale Mapping." *IEEE Geoscience and Remote Sensing Letters* 8: 426–430. doi:10.1109/LGRS.2010.2079913.

Linder, S. 1987. "Responses to Water and Nutrients in Coniferous Ecosystems." In *Potentials and Limitation of Ecosystems Analysis*, edited by E. D. Schulze and H. Z. Wolfer Ecol. Studies 61, pp. 180–202. New York: Springer-Verlag.

Liu, J., A. K. Skidmore, S. Jones, T. Wang, M. Heurich, X. Zhu, and Y. Shi. 2018. "Large off-Nadir Scan Angle of Airborne LiDar Can Severely Affect the Estimates of Forest Structure Metrics." *ISPRS Journal of Photogrammetry and Remote Sensing* 136: 13–25. doi:10.1016/j.isprsjprs.2017.12.004.

Lovell, J. L., D. L. Jupp, D. S. Culvenor, and N. C. Coops. 2003. "Using Airborne and Ground-Based Ranging LiDar to Measure Canopy Structure in Australian Forests." *Canadian Journal of Remote Sensing* 29 (5): 607–622. doi:10.5589/m03-026.

Magnussen, S. and P. Boudewyn. 1998. "Derivations of Stand Heights from Airborne Laser Scanner Data with Canopy-Based Quantile Estimators." Canadian Journal of Forest Research 28 (7): 1016–1031. doi:10.1139/x98-078.

Moe, K. T., T. Owari, N. Furuya, and T. Hiroshima. 2020. "Comparing Individual Tree Height Information Derived from Field Surveys, LiDar and UAV-DAP for High-Value Timber Species in Northern Japan." *Forests* 11 (2): 223. doi:10.3390/f11020223.

Morsdorf, F., B. Kötz, E. Meier, K. I. Itten, and B. Allgöwer. 2006. "Estimation of LAI and Fractional Cover from Small Footprint Airborne Laser Scanning Data Based in Gap Fraction." *Remote Sensing of Environment* 104 (1): 50–61. doi:10.1016/j.rse.2006.04.019.

Morsdorf, F., E. Meier, B. Kötz, K. I. Itten, M. Dobbertin, and B. Allgöwer. 2004. "LIDAR-Based Geometric Reconstruction of Boreal Type Forest Stands at Single Tree Level for Forest and Wildland Fire Management." *Remote Sensing of Environment* 92 (3): 353–362. doi:10.1016/j.rse.2004.05.013.

Peduzzi, A., R. Wynne, T. Fox, R. F. Nelson, and V. Thomas. 2012. "Estimating Leaf Area Index in Intensively Managed Pine Plantations Using Airborne Laser Scanner Data." *Forest Ecology and Management* 270: 54–65. doi:10.1016/j.foreco.2011.12.048.

Plowright, A. and J. Roussel 2020. "ForestTools: Analyzing Remotely Sensed Forest Data. R Package Version 0.2.1." https://cran.r-project.org/web/packages/ForestTools/index.html

Popescu, S. C. and K. Zhao. 2008. "A Voxel-Based LiDar Method for Estimating Crown Base Height for Deciduous and Pine Trees." *Remote Sensing of Environment* 112 (3): 767–781. doi:10.1016/j.rse.2007.06.011.

Popescu, S. C. and R. H. Wynne. 2004. "Seeing the Trees in the Forest: Using LiDar and Multispectral Data Fusion with Local Filtering and Variable Window Size for Estimating Tree Height." Photogrammetric Engineering & Remote Sensing 70 (5): 589–604. doi:10.14358/PERS.70.5.589.

Popescu, S. C., R. H. Wynne, and J. A. Scrivani. 2004. "Fusion of Small-Footprint LiDar and Multispectral Data to Estimate Plot-Level Volume and Biomass in Deciduous and Pine Forests in Virginia, USA." *Forest Science* 50 (4): 551–565.

Popescu, S. C., R. H. Wynne, and R. F. Nelson. 2003. "Measuring Individual Tree Crown Diameter with Lidar and Assessing Its Influence on Estimating Forest Volume and Biomass." *Canadian Journal of Remote Sensing* 29 (5): 564–577. doi:10.5589/m03-027.

R Core Team. 2021. *R: A Language and Environment for Statistical Computing*. Vienna, Austria: R Foundation for Statistical Computing.

Riaño, D., F. Valladares, S. Condés, and E. Chuvieco. 2004. "Estimation of Leaf Area Index and Covered Ground from Airborne Laser Scanner (LiDar) in Two Contrasting Forests." *Agricultural and Forest Meteorology* 124 (3): 269–275. doi:10.1016/j.agrformet.2004.02.005.

Roussel, J. R., D. Auty, N. C. Coops, P. Tompalski, T. R. H. Goodbody, A. Sánchez Meador, J. F. Bourdon, F. De Boissieu, and A. Achim. 2020. "lidR : An R Package for Analysis of Airborne Laser Scanning (ALS) Data." *Remote Sensing of Environment* 251: 112061. doi:10.1016/j.rse.2020.112061.

Roussel, J. R., J. Caspersen, M. Béland, S. Thomas, and A. Achim. 2017. "Removing Bias from LiDar-Based Estimates of Canopy Height: Accounting for the Effects of Pulse Density and Footprint Size." *Remote Sensing of Environment* 198: 1–16. doi:10.1016/j.rse.2017.05.032.

Sankey, T., J. Donager, J. McVay, and J. B. Sankey. 2017. "UAV Lidar and Hyperspectral Fusion for Forest Monitoring in the Southwestern USA." *Remote Sensing of Environment* 195: 30–43. doi:10.1016/j.rse.2017.04.007.

Schomaker, M. 2007. *Crown-Condition Classification: A Guide to Data Collection and Analysis*. Vol. 102. Asheville. NC: US Department of Agriculture, Forest Service, Southern Research Station.

Shao, G., S. C. Stark, D. R. de Almeida, and M. N. Smith. 2019. "Towards High Throughput Assessment of Canopy Dynamics: The Estimation of Leaf Area Structure in Amazonian Forests with Multitemporal Multi-Sensor Airborne Lidar." *Remote Sensing of Environment* 221: 1–13. doi:10.1016/j.rse.2018.10.035.

Silva, C. A., A. T. Hudak, L. A. Vierling, C. Klauberg, M. Garcia, A. Ferraz, M. Keller, J. Eitel, and S. Saatchi. 2017. "Impacts of Airborne Lidar Pulse Density on Estimating Biomass Stocks and Changes in a Selectively Logged Tropical Forest." *Remote Sensing* 9 (10): 1068. doi:10.3390/rs9101068.

Solberg, S., A. Brunner, K. H. Hanssen, H. Lange, E. Næsset, M. Rautiainen, and P. Stenberg. 2009. "Mapping LAI in a Norway Spruce Forest Using Airborne Laser Scanning." *Remote Sensing of Environment* 113 (11): 2317–2327. doi:10.1016/j.rse.2009.06.010.

Stenberg, P. 1996. "Correcting LAI-2000 estimates for the clumping of needles in shoots of conifers." *Agricultural and Forest Meteorology* 79 (1–2): 1–8.

Suárez, J. C., C. Ontiveros, S. Smith, and S. Snape. 2005. "Use of Airborne LiDar and Aerial Photography in the Estimation of Individual Tree Heights in Forestry." *Computers & Geosciences* 31 (2): 253–262. doi:10.1016/j.cageo.2004.09.015.

Sumnall, M. J., A. Trlica, D. R. Carter, R. L. Cook, M. L. Schulte, O. C. Campoe, R. A. Rubilar, R. H. Wynne, and V. A. Thomas. 2021. "Estimating the Overstory and Understory Vertical Extents and Their Leaf Area Index in Intensively Managed Loblolly Pine (Pinus Taeda L.) Plantations Using Airborne Laser Scanning." *Remote Sensing of Environment* 254: 112250. doi:10.1016/j.rse.2020.112250.

Sumnall, M. J., T. R. Fox, R. H. Wynne, C. Blinn, and V. A. Thomas. 2016. "Estimating Leaf Area Index at Multiple Heights Within the Understorey Component of Loblolly Pine Forests from Airborne Discrete-Return Lidar." *International Journal of Remote Sensing* 37 (1): 78–99. doi:10.1080/01431161.2015.1117683.

Trimble. 2003. "Trimble R7/R8 GPS Receiver-User Guide." Accessed 23 November 2021. https://www.ngs.noaa.gov/corbin/class_description/TrimbleR7-R8_UserGuide.pdf

Vasilescu, M.M. 2013. "Standard error of tree height using Vertex III. Bulletin of the Transilvania University of Brasov." *Forestry, Wood Industry, Agricultural Food Engineering. Series* II 6 (2): 75.

Vauhkonen, J., L. Ene, S. Gupta, J. Heinzel, J. Holmgren, J. Pitkänen, and S. Solberg et al. 2012. "Comparative Testing of Single-Tree Detection Algorithms Under Different Types of Forest." *Forestry* 85 (1): 27–40. doi:10.1093/forestry/cpr051.

Velodyn. 2019. "VLP-16 User Manual, Velodyn." Accessed 9 November 2021. https://velodynelidar.com/wp-content/uploads/2019/12/63-9243-Rev-E-VLP-16-User-Manual.pdf

Venables, W. N. and B. D. Ripley 2002. *Modern Applied Statistics with S*. 4thed. New York: Springer.

Wallace, L., A. Lucieer, C. Watson, and D. Turner. 2012. "Development of a UAV-LiDar System with Application to Forest Inventory." *Remote Sensing* 4 (6): 1519–1543. doi:10.3390/rs4061519.

Wang, Y., J. Hyyppä, X. Liang, H. Kaartinen, X. Yu, E. Lindberg, and J. Holmgren et al. 2016. "International Benchmarking of the Individual Tree Detection Methods for Modeling 3-D Canopy Structure for Silviculture and Forest Ecology Using Airborne Laser Scanning." *IEEE Transactions on Geoscience and Remote Sensing* 54 (9): 5011–5027. doi:10.1109/TGRS.2016.2543225.

Welles, J. M. and J. M. Norman. 1991. "Instrument for Indirect Measurement of Canopy Architecture." *Agronomy Journal* 83 (5): 818–825. doi:10.2134/agronj1991.00021962008300050009x.

Yan, W., H. Guan, L. Cao, Y. Yu, C. Li, and J. Lu. 2020. "A Self-Adaptive Mean Shift Tree-Segmentation Method Using UAV LiDar Data." *Remote Sensing* 12 (3): 515. doi:10.3390/rs12030515.

Yáñez, M. A., J. R. Seiler, and T. R. Fox. 2017. "Crown Physiological Responses of Loblolly Pine Clones and Families to Silvicultural Intensity: Assessing the Effect of Crown Ideotype." *Forest Ecology and Management* 398: 25–36. doi:10.1016/j.foreco.2017.05.002.

Yáñez, M.A., T.R. Fox, and J.R. Seiler. 2015. "Early growth responses of loblolly pine varieties and families to silvicultural intensity." *Forest Ecology and Management* 356: 204–215 doi:10.1016/j.foreco.2015.07.013.

Yao, W., J. Krull, P. Krzystek, and M. Heurich. 2014. "Sensitivity Analysis of 3D Individual Tree Detection from LiDar Point Clouds of Temperate Forests." *Forests* 5 (6): 1122–1142. doi:10.3390/f5061122.

Yu, X., A. Kukko, H. Kaartinen, Y. Wang, X. Liang, L. Matikainen, and J. Hyyppä. 2020. "Comparing Features of Single and Multi-Photon Lidar in Boreal Forests." *ISPRS Journal of Photogrammetry and Remote Sensing* 168: 268–276. doi:10.1016/j.isprsjprs.2020.08.013.

Zhao, K. and S. Popescu. 2009. "Lidar-Based Mapping of Leaf Area Index and Its Use for Validating GLOBCARBON Satellite LAI Product in a Temperate Forest of the Southern USA." *Remote Sensing of Environment* 113 (8): 1628–1645. doi:10.1016/j.rse.2009.03.006.